Chinese Chemical Letters 34 (2023) 108520

Contents lists available at ScienceDirect

Chinese Chemical Letters

journal homepage: www.elsevier.com/locate/cclet

Cu/$CdCO_3$ catalysts for efficient electrochemical CO_2 reduction over the wide potential window

Congwen Sun[a], Jinhui Hao[a], Bing Wei[b], Meng Wu[a], Hong Liu[a], Yusong Xiong[a], Bochen Hu[a], Longhua Li[a], Min Chen[a,*], Weidong Shi[a,*]

[a] School of Chemistry and Chemical Engineering, Jiangsu University, Zhenjiang 212013, China
[b] School of Resource and Environmental Engineering, Jilin Institute of Chemical Technology, Jilin 132000, China

ARTICLE INFO

Article history:
Received 28 February 2023
Revised 23 April 2023
Accepted 25 April 2023
Available online 28 April 2023

Keywords:
OH^-
Local pH
Inhibition of hydrogen evolution
CO
Wide potential window

ABSTRACT

High efficiency and low-cost catalyst-driven electrocatalytic CO_2 reduction to CO production are of great significance for energy storage and development. The severe competitive hydrogen evolution reaction occurs at large negative potential window limits the achievement of the target product from CO_2 at high efficiency. Here, we successfully prepared $Cu_x/CdCO_3$ composite catalyst rich in interfaces, in which achieved high CO Faraday efficiency exceeded 90% in a wide potential window of 700 mV and highest value up to 97.9% at −0.90 V *vs.* RHE. The excellent performance can be ascribed to the positive contribution of $Cu_x/CdCO_3$, which maintains a suitable high local pH value during electrochemical reduction, thus inhibiting the competitive hydrogen evolution reaction. Moreover, the compact structure between Cu and $CdCO_3$ ensures fast electron transfer both inside catalysts and interface, thus speeding up the reaction kinetics of CO_2 to CO conversion. Theoretically calculations further prove that the combination of Cu and $CdCO_3$ provides the well-defined electronic structure for intermediates adsorption, significantly reducing the reaction barrier for the formation of CO. This work provides new insights into the design of efficient electrochemical CO_2 reduction catalysts for inhibiting hydrogen evolution by adjusting the local pH effect.

Using renewable energy generated electricity to drive the electrocatalytic reduction of CO_2 into valuable chemicals is an effective way to reduce the greenhouse effect and solve the energy crisis [1]. The electrochemical CO_2 reduction reaction (CO_2RR) involves multiple steps of electron and proton transfer, so multiple products can be produced [2]. Among the various products of the electrochemical CO_2RR, CO is favored because it is an important ingredient in many chemical reactions [3]. Hydrogen evolution reaction (HER) is a strong competitive reaction of CO_2RR [4], especially under the relatively negative potential. At a more negative potential, due to the limitation of CO_2 mass transfer [5], hydrogen (H_2) is more easily generated, so highly selective electrochemical CO_2 reduction can only take place in a narrow potential window. Therefore, it is of great significance to develop a catalyst that can inhibit hydrogen (H_2) evolution at a more negative potential for realizing the electrochemical reduction of CO_2 to CO under a wide potential window.

Transition metal Cd-based catalysts have been widely studied due to their low cost and good performance in inhibiting H_2 evolution [6,7]. $CdCO_3$ in the Cd-based catalyst had the ability to activate CO_2 because it contained C atoms, which could combine with O in CO_2 [7]. Nevertheless, the activity of $CdCO_3$ for CO_2 reduction to CO was not satisfactory, which could only be greater than 90% under a narrow potential window (<300 mV). Experimental and theoretical studies showed that the construction of heterostructure was one of the key strategies to improve the selectivity of CO_2RR products [8]. Heterostructure interfaces with abundant active sites accelerated the electron transport and regulated the adsorption barrier of intermediates [9,10]. For instance, the recent research indicated $CdCO_3$/Cd-CP heterostructure interfaces reduced the energy barrier of the *COOH intermediate, thus realizing the highly selective reduction of CO_2 to CO under a 500 mV wide potential window [10]. Although many efforts have been made, the highly selective (>90%) electrochemical reduction of CO_2 to CO over $CdCO_3$ catalysts at a potential window was greater than 500 mV has not been reported.

Recently, the microenvironment near the electrode has been proved to have a great influence on the selectivity of CO_2RR [11]. Raising the local pH near the electrode was of great benefit to in-

* Corresponding authors.
E-mail addresses: chenmin3226@sina.com (M. Chen), swd1978@ujs.edu.cn (W. Shi).

https://doi.org/10.1016/j.cclet.2023.108520
1001-8417/

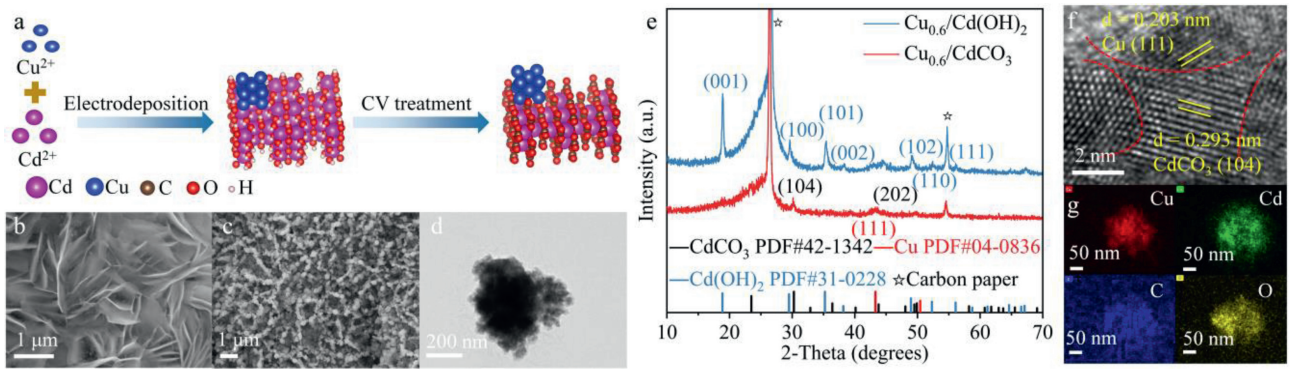

Fig. 1. (a) Schematic diagram of preparing $Cu_x/CdCO_3$ electrocatalysts. SEM image of the (b) $Cu_{0.6}/Cd(OH)_2$ and (c) $Cu_{0.6}/CdCO_3$. (d) TEM image of the $Cu_{0.6}/CdCO_3$. (e) XRD patterns of the $Cu_{0.6}/Cd(OH)_2$ and $Cu_{0.6}/CdCO_3$. (f) HRTEM image and (g) EDS-mapping images of the $Cu_{0.6}/CdCO_3$.

hibit HER, thus improving the selectivity of CO_2RR [12,13]. Luo *et al*. suppressed the formation of H_2 by using the OH^- formed *in-situ* preparation of rhombohedral $CdCO_3$ crystal (i-$CdCO_3$), and realized the highly selective reduction of CO_2 to CO under 500 mV wide potential window [13]. However, the high current density of CO_2RR would lead to the OH^- concentration near the electrode being many orders of magnitude higher than the bulk solution [14,15]. Excessive concentration of OH^- would react with CO_2 to generate CO_3^{2-}, which was not conducive to inhibition of HER [16]. Therefore, adjusting the concentration of OH^- near the electrode to maintain an appropriate local pH value was particularly important for inhibiting HER and further improved the selectivity of the catalyst for CO_2 reduction.

Here, we have enhanced the potential window of highly selective reduction of CO_2 to CO by combining the construction of heterostructure with the regulation of local pH. By adjusting the feed ratio of Cu^{2+} and Cd^{2+}, the ability of the electrode to produce OH^- and adsorb OH^- could be adjusted. When the ratio of Cu^{2+}/Cd^{2+} metal ions was 6:4, the catalyst exhibited the FE_{co} exceeded 90% under the wide potential window of 700 mV and the highest FE_{co} of 97.9% at −0.90 V (*vs.* RHE). Moreover, $Cu_{0.6}/CdCO_3$ showed excellent hydrogen evolution inhibition performance. The experimental results showed that an appropriate high local pH near the electrode inhibited the HER, and $Cu_x/CdCO_3$ composite structure created more active sites for electrochemical reduction of CO_2 to CO. The density functional theory (DFT) calculations also revealed that the excellent reduction of CO_2 to CO came from the adjustment of the local electronic structure of adjacent metal active sites by the $Cu_x/CdCO_3$ composite structure, which reduced the formation barrier of *CO intermediates.

The synthesis of the catalyst was shown in Fig. 1a. Firstly, $Cu_x/Cd(OH)_2$ was prepared directly on carbon paper by using a one-step co-deposition method [17], where x represented the molar mass of Cu as a percentage of the total metal ion. Next, the $Cu_x/CdCO_3$ working electrode was prepared by cyclic voltammetry (CV) conversion in CO_2-saturated 0.1 mol/L $KHCO_3$. The microstructure of $Cu_{0.6}/Cd(OH)_2$ and $Cu_{0.6}/CdCO_3$ could be obtained from scanning electron microscope (SEM) and transmission electron microscopy (TEM) measurements (Figs. 1b-d). It could be seen that after the CV treatment, the morphology changed from nanosheets to irregular particles. X-ray diffraction (XRD) directly proved the transition from $Cu_{0.6}/Cd(OH)_2$ to $Cu_{0.6}/CdCO_3$, indicating the successful preparation of the composite catalyst (Fig. 1e). High-resolution TEM images (Fig. 1f) showed interfacial distances of 0.293 and 0.203 nm, which were consistent with (104) plane of $CdCO_3$ [18] and (111) plane of Cu [19], respectively. The element mapping image also showed that Cu, Cd, O, and C species were evenly distributed on the carbon paper (Fig. 1g). The measurement

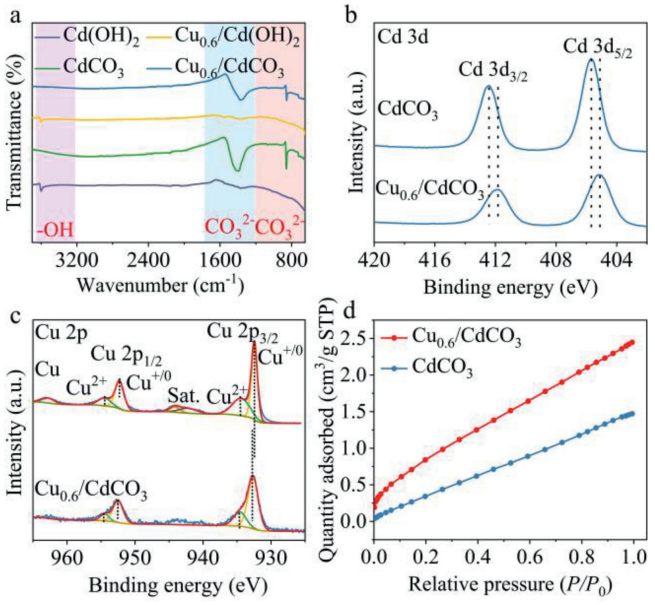

Fig. 2. (a) FT-IR spectra of the $Cd(OH)_2$, $CdCO_3$, $Cu_{0.6}/Cd(OH)_2$ and $Cu_{0.6}/CdCO_3$. (b) Cd 3d XPS spectra of $CdCO_3$ and $Cu_{0.6}/CdCO_3$. (c) Cu 2p XPS spectra of Cu and $Cu_{0.6}/CdCO_3$. (d) CO_2 adsorption curves of $Cu_{0.6}/CdCO_3$ and $CdCO_3$ at 273.15 K.

of lattice fringes and the uniform distribution of elements further indicated the successful preparation of a composite catalyst.

Fourier transform infrared (FT-IR) spectra of the samples before and after CV treatment was used to further demonstrate the successful carbonate transition (Fig. 2a). The disappearance of OH stretching vibration peak and the appearance of anti-symmetric stretching vibration peak and off-plane bending vibration absorption peak of CO_3^{2-} further proved the successful preparation of $Cu_{0.6}/CdCO_3$ [20,21]. The valence states of Cu and Cd on $Cu_x/CdCO_3$ surfaces were characterized by X-ray photoelectron spectroscopy (XPS). Compared with $Cu_{0.6}/CdCO_3$, the double peaks of Cd 3d in the $CdCO_3$ had a larger binding energy shift of 0.5 eV (Fig. 2b). On the contrary, the Cu 2p binding energy in Cu shifted to a smaller direction than that in $Cu_{0.6}/CdCO_3$ (Fig. 2c) [22]. XPS results demonstrated that there was a strong interaction between the electronic structures of Cu and Cd [23]. In addition, CO_2 adsorption capacity (Fig. 2d) tests were used to analyze the structural properties of the materials. The adsorption capacity of $Cu_{0.6}/CdCO_3$ for CO_2 was 2.45 cm^3/g STP and 1.70 times that of $CdCO_3$ (1.44 cm^3/g STP) (Fig. 2d). Stronger CO_2 adsorption capacity was conducive to subsequent CO_2 reduction [24].

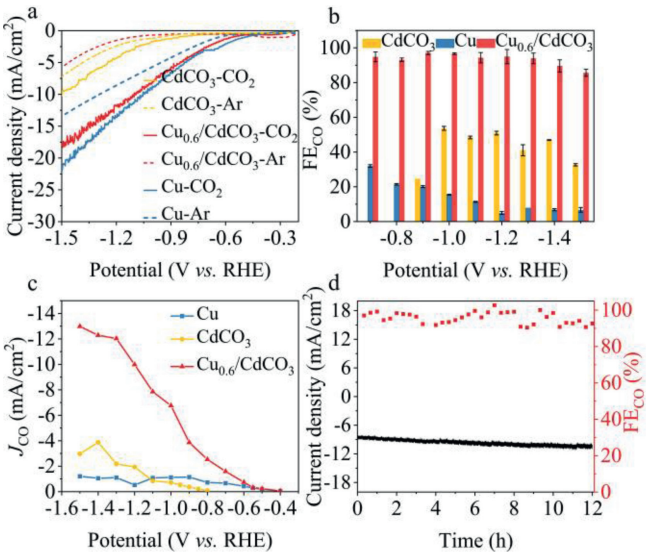

Fig. 3. (a) LSV of the Cu, $CdCO_3$ and $Cu_{0.6}/CdCO_3$. (b) FE_{co} of the $CdCO_3$, Cu and $Cu_{0.6}/CdCO_3$. (c) Comparison of CO fractional current densities of $CdCO_3$, Cu and $Cu_{0.6}/CdCO_3$. (d) Stability test of $Cu_{0.6}/CdCO_3$ at −1.20 V *vs.* RHE.

Fig. 3a showed the linear sweep voltammetry curves (LSV) of $Cu_{0.6}/CdCO_3$, $CdCO_3$, and Cu in Ar and CO_2-saturated 0.1 mol/L $KHCO_3$ solutions, respectively. The current density in CO_2-saturated 0.1 mol/L $KHCO_3$ solutions was higher than that in Ar-saturated 0.1 mol/L $KHCO_3$ solutions, which preliminarily showed that the catalyst could electrochemically reduce of CO_2. According to researches, Cu was a post transition metal with low resistance and good conductivity [25]. $CdCO_3$, which belonged to the metal carbonate class, had a large resistance and a slow electron transfer rate compared to metals [26]. Therefore, at the same potential, $CdCO_3$ had the lowest current density in CO_2-saturated 0.1 mol/L $KHCO_3$ solution, while Cu exhibited the highest current density. The current density of catalysts with different proportions gradually increased with the increase of Cu content (Fig. S5 in Supporting information). The performance of the catalyst for CO_2 reduction under different applied potentials was tested by constant potential method. The Faraday efficiency (FE) of CO for $Cu_{0.6}/CdCO_3$ exceeded 90% in potential windows ranging from −0.70 V to −1.40 V (*vs.* RHE) and reached a maximum value of 97.9% at −0.90 V (*vs.* RHE) (Fig. 3b). By testing the CO selectivity of other samples with different proportions, it was found that the CO selectivity first increased and then decreased with the increase of Cu content, and reached the highest value when the Cu content was 60% (Fig. S7 in Supporting information).

In addition to FE, current density, energy conversion efficiency, and stability were also important indicators to evaluate the catalytic performance of CO_2RR. $Cu_{0.6}/CdCO_3$ had a superior CO component current density, which could reach a large value of 12.98 mA/cm^2 at −1.50 V (*vs.* RHE) potential (Fig. 3c). This was far more than the CO component current density of $CdCO_3$ (2.98 mA/cm^2) and Cu (1.21 mA/cm^2), indicating that it had an excellent catalytic activity of CO_2 reduction to CO. Moreover, according to the current density and potential function diagram generated by CO (Fig. 3c), when $Cu_{0.6}/CdCO_3$ generated CO, the overpotential required had a positive displacement of about 400 mV compared with that required by $CdCO_3$. These results showed that the composite structures could both increase the current density and reduce the overpotential of electrocatalytic CO_2 reduction to produce CO. Furthermore, $Cu_{0.6}/CdCO_3$ had outstanding cathode energy efficiency, which could reach 67.8% at −0.70 V (Fig. S8b in Supporting information).

Long-term experiments were used to evaluate its stability. The electrodes were tested at a potential of −1.20 V *vs.* RHE (8.56 mA/cm^2) for up to 12 h. As shown in Fig. 3d, the current density dropped slightly during the 12-h test, but the Faraday efficiency was still greater than 90%. The SEM (Fig. S13 in Supporting information), XRD (Fig. S14 in Supporting information), and XPS (Fig. S15 in Supporting information) of the samples did not change significantly before and after the long-term stability test. Therefore, $Cu_{0.6}/CdCO_3$ was a promising catalyst with excellent activity, high CO selectivity, and long-term stability.

To better understand the source of the enhanced catalyst activity, the electrochemically active surface area (ECSA) was analyzed by testing the double-layer capacitance (C_{dl}) [27]. The C_{dl} value of $Cu_{0.6}/CdCO_3$ was 9.23 mF/cm^2 (Fig. 4a), 18 and 1.56 times higher than that of $CdCO_3$ (0.51 mF/cm^2), and Cu (5.90 mF/cm^2), respectively, indicating its abundant active sites on the surface. This result was consistent with the activity of CO_2RR. Furthermore, an electrochemical impedance spectroscopy (EIS) test was performed at the potential of −0.90 V (*vs.* RHE) to analyze the electron transfer resistance between the catalyst and the electrolyte [28]. Nyquist diagram showed that the charge transfer resistance and material transfer resistance of $Cu_{0.6}/CdCO_3$ were much smaller than that of $CdCO_3$ (Fig. 4b). Less resistance was beneficial to the rapid transfer of electrons and the substances [29,30], which could further promote the formation of intermediates in CO_2RR. The Tafel curve measurement (Fig. S10 in Supporting information) was used to study the dynamics of the CO_2RR process. Compared to Cu (181 mV/dec), $CdCO_3$ (259 mV/dec), and other ratios of $Cu_x/CdCO_3$ catalysts, $Cu_{0.6}/CdCO_3$ had the smallest Tafel slope (134 mV/dec). The Tafel slope of $Cu_{0.6}/CdCO_3$ was close to 118 mV/dec, indicating that the first electron transfer to CO_2 to generate CO_2^- was a rate-determining step (RDS) [31]. The minimum Tafel slope also meant faster CO formation kinetics [32].

A rotating disk electrode was used to directly measured the OH^- generated near the electrode [33]. As the applied potential on the disk increases, CO oxidation peak (E_{obs}) moved in a more negative direction (Fig. S12 in Supporting information), which directly proved the generation of OH^- on the electrode. According to the LSV of samples with different proportions, the current density of the sample increased with the increase of Cu content, which meant that the ability to produce OH^- was also proportional to the Cu content. At the same time, the oxidation test curve in Ar-saturated 0.1 mol/L KOH solution was used to test the overpotential required for OH^- adsorption (Fig. 4c). The results showed that the overpotential of OH^- adsorption decreased with the increase of Cu content, which meant that the introduction of Cu could enhance the adsorption of OH^- [34]. Further comparing the selectivity of different catalysts for H_2, it was found that $Cu_{0.6}/CdCO_3$ had the lowest selectivity for H_2 over the entire tested potential range (Fig. S7 in Supporting information). Therefore, the pH value of $Cu_{0.6}/CdCO_3$ surface was optimal, which was more conducive to inhibition of HER. To further study the effect of local pH on CO_2RR, the CO_2RR of $Cu_{0.6}/CdCO_3$ and $CdCO_3$ were tested at a constant current density of 2.71 mA/cm^2 at 0.05 mol/L K_2HPO_4, 0.1 mol/L $KHCO_3$ and 0.1 mol/L KCl, respectively [12]. The buffering capacity of K_2HPO_4, $KHCO_3$, and KCl decreased in turn, while the local pH value increased in turn. As shown in Fig. 4d, with the increase of local pH, the FE_{H_2} became lower, and the FE_{co} became higher. This further proved that moderately high local pH was favorable for CO_2RR and unfavorable for HER.

In-situ Raman spectroscopy (Fig. 4e) was used to test the reaction path of electrochemical reduction of CO_2 to CO by $Cu_{0.6}/CdCO_3$. The peak at 250 cm^{-1} was attributed to the Cu-CO stretching mode [35], which became stronger with the increase of potential. The peaks at 523 and 1030 cm^{-1} were attributed to Cu_xO [35] and *OCO intermediate [36]. After protonation, the *OCO

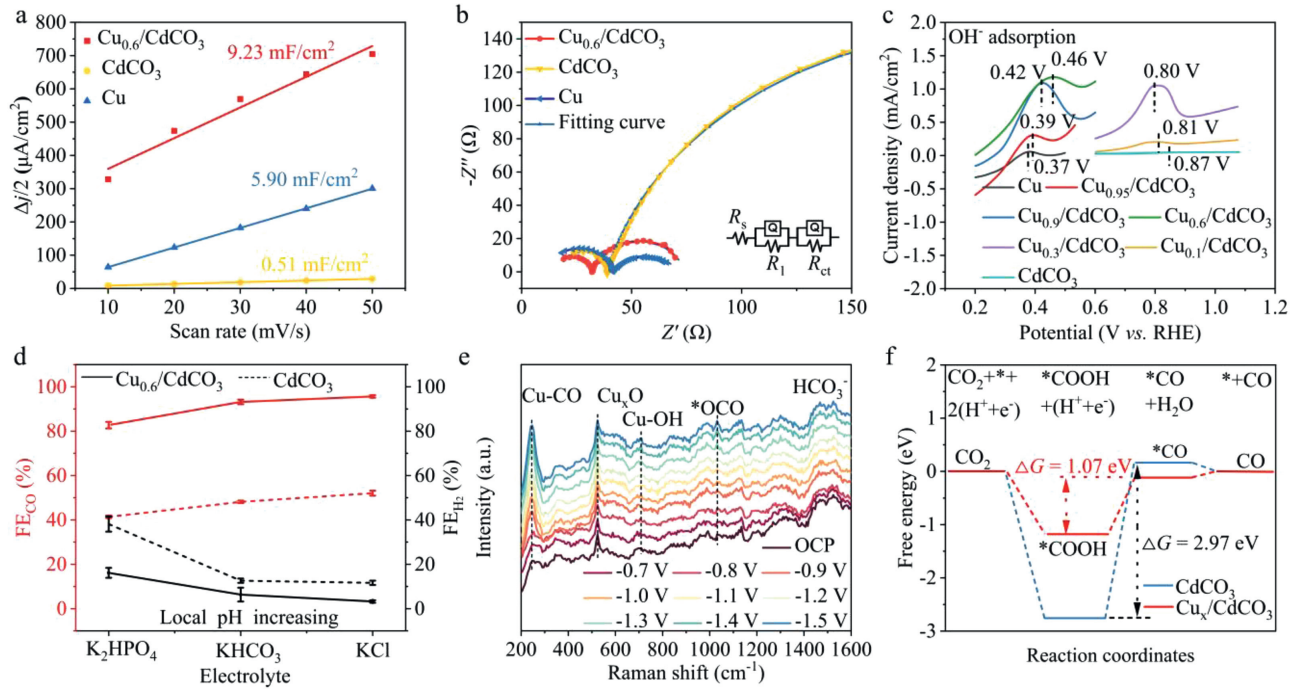

Fig. 4. (a) Current density differences ($\Delta j/2$) plotted against scan rates of the Cu, $CdCO_3$ and $Cu_{0.6}/CdCO_3$. (b) Nyquist plots. (c) Oxidative LSV curves in Ar-saturated 0.1 mol/L KOH electrolyte of $Cu_x/CdCO_3$. (d) pH-dependence experiment on $Cu_{0.6}/CdCO_3$ (solid line) and $CdCO_3$ (dotted line) in 0.05 mol/L K_2HPO_4, 0.1 mol/L $KHCO_3$, 0.1 mol/L KCl solution at 2.71 mA/cm^2. (e) *In-situ* Raman diagram of $Cu_{0.6}/CdCO_3$ at different potentials. (f) Free energy diagrams of each intermediate during the electrochemical reduction of CO_2 to CO on the $Cu_x/CdCO_3$ and $CdCO_3$.

intermediate was transformed into *OCHO, which was conducive to the formation of HCOOH [36]. According to the *in-situ* Raman results, the peak of *OCO was obvious at high potential (<−1.20 V *vs.* RHE), indicating that a small amount of HCOOH was generated at high potential, which was consistent with our experimental results. The Cu-OH peak at 706 cm^{-1} appeared from the −0.70 V *vs.* RHE [37]. When the applied potential was less than −1.20 V *vs.* RHE, the peak became more obvious. This directly proved the existence of OH^- on the surface of the catalyst and further validated the local pH rise. The DFT calculation was performed to further analyze the active source of $Cu_x/CdCO_3$ for high selectivity CO_2RR. The calculated Gibbs free energy (ΔG) diagram of each intermediate was shown in Fig. 4f. On the surface of $Cu_x/CdCO_3$, the ΔG required for the transition from *COOH to *CO was 1.07 eV, which was much smaller than the 2.97 eV of $CdCO_3$. This indicated that $Cu_x/CdCO_3$ was more conducive to the formation of *CO [38]. The d-band center was the key to determining the electrochemical activity, which could be evaluated by partial state density (PDOS) data [39]. Compared with $CdCO_3$, the d-band center of Cd in $Cu_x/CdCO_3$-*COOH was closer to the Fermi level, while the d-band center of Cd in $Cu_x/CdCO_3$-*CO was further away from the Fermi level (Fig. S19 in Supporting information). This proved that the $Cu_x/CdCO_3$ surface had a strong adsorption energy for *COOH and a weak adsorption energy for *CO [40]. These results showed that the strong electron interaction between Cu and $CdCO_3$ could reduce the formation energy barrier of *CO intermediate and promote the desorption of CO from $Cu_x/CdCO_3$ surface, so that the electrochemical CO_2 reduction to CO had a fast reaction kinetics.

In summary, $Cu_x/CdCO_3$ catalysts were prepared for the first time by simple electrodeposition and CV treatment. $Cu_{0.6}/CdCO_3$ exhibited excellent performance of reducing CO_2 to CO, high CO partial current density and fine stability. The experimental results proved that the excellent performance of $Cu_{0.6}/CdCO_3$ catalyst came from the reasonable adjustment of OH^- generation and adsorption, which inhibited HER. Theoretical calculations have proved that $Cu_x/CdCO_3$ catalyst reduced the energy barrier from *COOH to *CO intermediate, thus realizing the highly selective electrochemical reduction of CO_2 to CO under a wide potential window. This work explored the influence of local microenvironment and electronic structure on the CO_2RR, which will provide new guidance for the design of highly selective electrocatalysts under a wide potential window.

Declaration of competing interest

The authors declare that they have no known competing financial interests or personal relationships that could have appeared to influence the work reported in this paper.

Acknowledgments

This work was supported by the National Natural Science Foundation of China (Nos. 22225808, 22075111), Sino–German Cooperation Group Project (No. GZ1579), Jiangsu Province Innovation Support Program International Science and Technology Cooperation Project (No. BZ2022045).

Supplementary materials

Supplementary material associated with this article can be found, in the online version, at doi:10.1016/j.cclet.2023.108520.

References

[1] S.I. Seneviratne, M.G. Donat, A.J. Pitman, R. Knutti, R.L. Wilby, Nature 529 (2016) 477–483.
[2] K.P. Kuhl, E.R. Cave, D.N. Abram, T.F. Jaramillo, Energy Environ. Sci. 5 (2012) 7050–7059.
[3] X. Chen, W. Zhang, W. Huang, Chin. Chem. Lett. 34 (2023) 107809.
[4] K. Xu, S. Zheng, Y. Li, et al., Chin. Chem. Lett. 33 (2022) 424–427.
[5] D. Raciti, M. Mao, J.H. Park, C. Wang, J. Electrochem. Soc. 165 (2018) F799.

[6] C. Wang, M. Cao, X. Jiang, M. Wang, Y. Shen, Electrochim. Acta 271 (2018) 544–550.
[7] X. Jiang, X. Wang, Q. Wang, et al., ACS Appl. Energy Mater. 4 (2021) 2073–2080.
[8] J. Sun, W. Zheng, S. Lyu, et al., Chin. Chem. Lett. 31 (2020) 1415–1421.
[9] D. Gao, Y. Zhang, Z. Zhou, et al., J. Am. Chem. Soc. 139 (2017) 5652–5655.
[10] J. Yang, H. Yang, R. Zhang, et al., J. Mater. Chem. A 10 (2022) 23028–23036.
[11] M. Ma, K. Djanashvili, W.A. Smith, Angew. Chem. Int. Ed. 55 (2016) 6680–6684.
[12] J.H. Zhou, K. Yuan, L. Zhou, et al., Angew. Chem. Int. Ed. 58 (2019) 14197–14201.
[13] J. Xiao, S. Liu, P.F. Sui, et al., Chem. Eng. J. 433 (2022) 133785.
[14] N. Gupta, M. Gattrell, B. MacDougall, J. Appl. Electrochem. 36 (2005) 161–172.
[15] B.M. Tackett, D. Raciti, N.W. Brady, N.L. Ritzert, T.P. Moffat, J. Phys. Chem. C 126 (2022) 7456–7467.
[16] B.R.W. Pinsent, L. Pearson, F.J.W. Roughton, Trans. Faraday Soc. 52 (1956) 1512–1520.
[17] Y. Xiong, B. Wei, M. Wu, et al., J. CO_2 Util. 51 (2021) 101621.
[18] J. Xiao, M.R. Gao, J.L. Luo, J. Power Sources 510 (2021) 230433.
[19] T. Feng, J. Wang, Y. Wang, et al., Chem. Eng. J. 433 (2022) 133495.
[20] A. Askarinejad, A. Morsali, Mater. Lett. 62 (2008) 478–482.
[21] L.A. Saghatforoush, S. Sanati, R. Mehdizadeh, M. Hasanzadeh, Superlattices Microstruct 52 (2012) 885–893.
[22] S. Kuang, M. Li, X. Chen, et al., Chin. Chem. Lett. 34 (2023) 108013.
[23] L. Gao, X. Zhong, J. Chen, et al., Chin. Chem. Lett. 34 (2023) 108085.
[24] G. Si, X. Kong, T. He, et al., Chin. Chem. Lett. 32 (2021) 918–922.
[25] Y. Hori, H. Wakebe, T. Tsukamoto, O. Koga, Electrochim. Acta 39 (1994) 1833–1839.
[26] R. Zhang, Q. Fu, P. Gao, et al., J. Energy Chem. 70 (2022) 95–120.
[27] B. Wei, Y. Xiong, Z. Zhang, et al., Appl. Catal. B 283 (2021) 119646.
[28] L. Xu, Z. Wang, X. Chen, et al., Electrochim. Acta 260 (2018) 898–904.
[29] J. Zhang, Y. Wang, H. Wang, D. Zhong, T. Lu, Chin. Chem. Lett. 33 (2022) 2065–2068.
[30] J. Hao, W. Yang, Z. Peng, et al., ACS Catal. 7 (2017) 4214–4220.
[31] S. Zhang, P. Kang, S. Ubnoske, et al., J. Am. Chem. Soc. 136 (2014) 7845–7848.
[32] S. Liu, H. Tao, L. Zeng, et al., J. Am. Chem. Soc. 139 (2017) 2160–2163.
[33] F. Zhang, A.C. Co, Angew. Chem. Int. Ed. 59 (2020) 1674–1681.
[34] A. Salehi−Khojin, H.R.M. Jhong, B.A. Rosen, et al., J. Phys. Chem. C 117 (2013) 1627–1632.
[35] T.T.H. Hoang, S. Verma, S. Ma, et al., J. Am. Chem. Soc. 140 (2018) 5791–5797.
[36] W. Shan, R. Liu, H. Zhao, et al., ACS Nano 14 (2020) 11363–11372.
[37] X. Chang, Y. Zhao, B. Xu, ACS Catal. 10 (2020) 13737–13747.
[38] H. Xue, H. Zhu, J. Huang, P. Liao, X. Chen, Chin. Chem. Lett. 34 (2023) 107134.
[39] W. Yang, J. Li, X. Cui, et al., Chin. Chem. Lett. 32 (2021) 2489–2494.
[40] Y. Sun, S. Wang, D. Jiao, et al., Chin. Chem. Lett. 33 (2022) 3987–3992.